J. Biochem. 126, 859-865 (1999)

Secondary Structures and Structural Fluctuation in a Dimeric Protein, *Streptomyces* Subtilisin Inhibitor[1]

Hiroaki Sasakawa,* Atsuo Tamura,*,[2] Shinichi Fujimaki,* Seiichi Taguchi,† and Kazuyuki Akasaka*

*Graduate School of Science and Technology, Kobe University, 1-1 Rokkodai-cho, Nada-ku, Kobe 657-8501; and †Polymer Chemistry Laboratory, RIKEN, 2-1 Hirosawa, Wako, Saitama 351-0198

Received July 28, 1999; accepted August 17, 1999

Based on the nuclear magnetic resonance assignments of a dimeric protein, *Streptomyces* subtilisin inhibitor (SSI), microscopic details of secondary structures in solution have been elucidated. The chemical shift index of C^{α} signals, together with information on the hydrogen exchange rates of the backbone amide protons, were used to identify secondary structures. The locations of these secondary structures were found to be different in some critical points from those determined earlier by X-ray crystallography of the crystal. Notably, the β3 strand is completely missing and the α2 helix is extended toward the C-terminus. Furthermore, hydrogen exchange experiments of individual peptide NH protons under strongly folding conditions revealed mechanisms of global and local structural fluctuation within the dimeric structure. It has been suggested that the global fluctuation of the monomeric unit occurs without affecting the accompanying monomer, in contrast to the equilibrium thermal unfolding, which is cooperative. Higher protection against hydrogen exchange for residues in part of the β4 strand implies that this region might serve as a folding core.

Key words: dimer, hydrogen exchange, protein dynamics, protein folding, secondary structure.

Streptomyces subtilisin inhibitor (SSI) (*1, 2*) is one of the most well-characterized proteins in terms of its crystallographic structure (*3-5*), thermodynamic properties (*6, 7*), and interactions with target enzymes (*8, 9*). The crystal structure of SSI retains a unique dimeric structure with two identical subunits associated through a β-sheet; each subunit consists of 113 amino acids with two disulfide bridges (*4*, Fig. 1). The subunits of SSI dissociate into denatured monomers upon denaturation without the accumulation of any monomeric native or intermediate forms (*10-14*). Mutational effects on thermodynamic stability (*15-17*) have also been studied extensively. In particular, SSI and its mutant forms have been found to undergo cold denaturation in acidic aqueous environments, and the thermodynamic parameters associated with heat and cold denaturation have been examined in detail by circular dichroism, micro-calorimetry, and ^{1}H NMR spectroscopy (*10, 11, 14*). Mutational effects on the interaction with target enzymes have also been studied crystallographically (*8, 9*).

On the other hand, microscopic details of the structure in solution have been studied only to a limited degree, using such methods as fluorescence (*18*), ^{1}H (*19-22*), and ^{13}C NMR spectroscopy (*23, 24*). In this paper, we used multidimensional NMR techniques to elucidate for the first time the secondary structures of SSI in solution based on the chemical shift index of the C^{α} signals and the hydrogen exchange rates of the peptide NH protons. Complete NMR assignments of backbone ^{1}HN, ^{15}N, and ^{13}C signals have recently been reported (*25*), although the self-association of the molecules at high concentration (*26*) has hampered the total assignment of all side chain signals and complete determination of the structure by NMR.

It is well known that hydrogen exchange experiments, especially in combination with two-dimensional NMR techniques, can be successfully applied to protein folding studies (for a review, see Ref. *27*). This method, however, has mainly been applied to studies of monomeric proteins. To our knowledge, only two dimeric proteins have been subjected to hydrogen exchange study to investigate protein folding, *Bacillus subtilis* SPO1-enhanced transcription factor 1 (*28*) and the Jun leucine zipper domain (*29*), both of which are helical proteins. On the other hand, SSI has a dimeric interface consisting solely of β-sheet (Fig. 1). Therefore this study provides a unique opportunity to investigate β-sheet interactions between subunits. Since the dimeric interaction under equilibrium conditions has been extensively studied calorimetrically, and the thermodynamic parameters have been determined with exceptional accuracy (*13, 15*), comparison of these thermodynamic parameters with the present kinetic analyses is expected to

[1] This work was supported by Grants-in-Aid for Scientific Research from the Ministry of Education, Science, Sports and Culture of Japan (to A.T. and K.A.).

[2] To whom correspondence should be addressed. Phone/Fax: 078-803-5692, E-mail: atamuta@kobe-u.ac.jp

Abbreviations: CSI, chemical shift index; CT, constant time; NMR, nuclear magnetic resonance; SSI, *Streptomyces* subtilisin inhibitor.

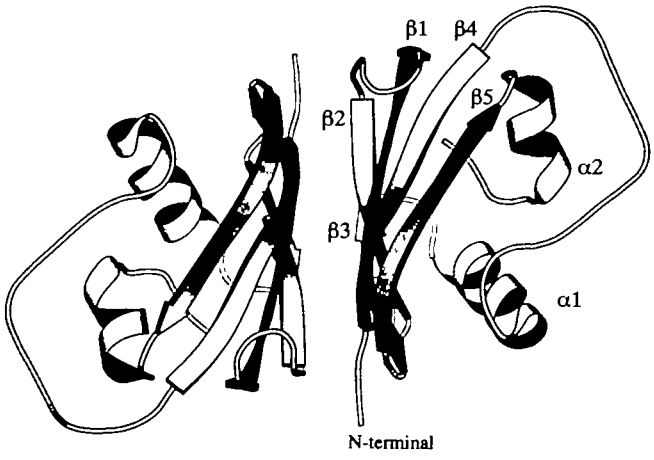

Fig. 1. **The tertiary structure of SSI generated with MOLSCRIPT (*47*) based on the crystallographic coordinates (*4*).**

shed light on the local and global structural fluctuation of the dimeric structure.

MATERIALS AND METHODS

Uniform Isotope Labeling—SSI uniformly labeled with ^{15}N or ^{13}C-^{15}N isotopes was produced by cultivating *E. coli* JM109 carrying pOST plasmid in M9 medium with $(^{15}NH_4)_2SO_4$ and ^{13}C-D-glucose as the only nitrogen and carbon sources, respectively. SSI uniformly labeled with ^{15}N isotopes was produced by cultivating *E. coli* JM109 carrying pOST plasmid in M9 medium with $(^{15}NH_4)_2SO_4$ as the only nitrogen source. After cultivating the *E. coli* for 24 h, the cells were harvested by centrifugation and subjected to the osmotic treatment. The resulting supernatant was precipitated with ammonium sulfate. The precipitate was dialyzed against 10 mM phosphate buffer, pH 7.0, through a Spectra/Por dialysis membrane (MWCO: 3,500, SPECTRUM). The dialysate was loaded onto an anion-exchange DEAE-Sepharose (DE52, Whatman) column equilibrated with 10 mM phosphate buffer, pH 7.0. The eluent was obtained by a linear gradient to 1 M NaCl (*2*), and the active fractions were dialyzed against 10 mM phosphate buffer, pH 7.0. The dialysate was applied to a gel filtration column (Sephacryl S-200 HR, Pharmacia). The fraction containing SSI was dialyzed against water and freeze-dried. Approximately 10 mg of electrophoretically pure SSI was obtained from 1 liter of culture broth.

Hydrogen Exchange Experiment—$^{13}C/^{15}N$-labeled SSI was dissolved in 95% ^1H_2O/5% ^2H_2O containing 25 mM phosphate buffer. For hydrogen exchange experiments, the ^{15}N-labeled protein samples were dissolved in 99.9% ^2H_2O containing 25 mM phosphate buffer, pH* 6.14, and in 99.9% ^2H_2O containing 25 mM borate buffer, pH* 8.96, at a concentration of 20 mg/ml. The pH* values cited are the direct readings of a pH meter without isotope correction.

All NMR measurements were performed on a Bruker DMX-750 spectrometer equipped with a triple resonance inverse probe with a field gradient unit. 3D CT-HNCA and CT-HN(CO)CA (*30, 31*) were measured for CSI analysis at 30°C, with a spectral width of 10,000 Hz in the ^1H axis, 2,000 Hz in the ^{15}N axis, and 2,000 Hz in the ^{13}C axis. The time domain signals were accumulated for a number of scans of eight into 1,024 complex data points for 64 t1 increments and for 64 t2 increments using WATERGATE for water suppression (*32*). Data processing and peak selection were carried out on SiliconGraphic workstations with nmrPipe, nmrDraw, and Pipp software (*33*). The ^1H chemical shifts were referenced to the methyl signal of DSS, while the ^{13}C and ^{15}N chemical shifts were referenced indirectly using the consensus γ_C/γ_H ratio of 0.25144954 and γ_N/γ_H ratio of 0.10132914 for ^{13}C and ^{15}N, respectively (*34*).

Hydrogen exchange reactions were followed on $^1H\{^{15}N\}$HSQC (*35*) spectra at pH* 8.96 and 6.14 at 52°C. Signal acquisition was started 5 min after the temperature was raised from 10 to 52°C at pH* 6.14. At pH* 8.96, acquisition was initiated after preincubation at 42°C for 12 h to completely exchange the labile hydrogens. The time-domain signals were collected into 2,048 complex data points for 128 t1 increments to a number of accumulations of 8. Spectral widths of 10,000 Hz and 2,584.6 Hz were employed in the ^1H and ^{15}N axes, respectively. The time domain data were processed with the XWINNMR software package (Bruker) on a SiliconGraphic workstation. To calculate the rates of hydrogen exchange, time dependent volume integrals of the amide proton signals were fitted to a single exponential function of time with the program Igor (Wave Metrics, Oregon) on a Macintosh computer.

Theory of Hydrogen-Deuterium Exchange and Its Application to a Dimeric Protein—Hydrogen exchange rates can be analyzed in terms of a structural unfolding model, in which exchange only takes place from an "open" form of the protein, but not from the "closed" form (*36*):

$$\text{N-H(closed)} \underset{k_f}{\overset{k_u}{\rightleftharpoons}} \text{N-H} \xrightarrow{k_{int}} \text{(open)N-D.} \quad (1)$$

In this scheme, k_u and k_f are the local unfolding and folding rates, respectively, and k_{int} is the intrinsic exchange rate for an amide proton in the open form. The sequence-specific intrinsic exchange rate for an amide proton, k_{int}, can be calculated for each protein by the method of Bai *et al.* (*37*). At the EX2 limit, *i.e.*, $k_u + k_f \gg k_{int}$, the measured exchange rate, k_{ex}, can be written as:

$$k_{ex} = k_u \times k_{int}/k_f = K_{op} \times k_{int} \quad (2)$$

where K_{op} is the equilibrium constant between the exchangeable open form and the non-exchangeable closed form of the hydrogen bond. In this case, protection factors (P) can be calculated from the measured exchange rates and the sequence-specific intrinsic exchange rates.

$$P = \frac{k_{int}}{k_{ex}} \quad (3)$$

The free energy for the equilibrium between the closed and open forms derived from the hydrogen exchange can be calculated as

$$\Delta G^{0ex} = -RT\ln(1/P) \quad (4)$$

On the other hand, when $k_u + k_f \ll k_{int}$,

$$k_{ex} \cong k_u \text{ (EX1 mechanism)} \quad (5)$$

Thus the observed rate constant reflects the rate of unfolding of the whole protein, k_u.

This theory can be applied to a dimeric protein by substituting $K_{op} = [\text{N-H(open)}]/[\text{N-H(closed)}]$ with $K_{op} =$

$[N\text{-}H(open)]^2/[N\text{-}H(closed)_2]$, where N-H(open) denotes an exchangeable monomeric form and $N\text{-}H(closed)_2$ represents a non-exchangeable dimeric form. Then the observed rate constants at the EX2 and EX1 limits can be derived according to the same formula as in Eqs. 2 and 5.

RESULTS

Chemical Shifts of the C^α Signal—The Chemical Shift Index (CSI) proposed by Wishert and Sykes (*38*), based on the differences in the chemical shifts of the Cα and signals from the corresponding random-coil values, were calculated for each residue of SSI and are shown plotted in Fig. 2, where +1 indicates a tendency toward α-helix and −1 indicates a tendency toward β-strand. The criterion for +1 or −1 is that the difference is higher than 0.8 ppm or lower than −0.5 ppm, respectively. Based on Fig. 2, we predict the existence of secondary structures of SSI as follows: β1, β2, α1, β4 , β5, and α2 for residues 10-16, 30-36, 46-55, 78-81, 89-98 and 100-110, respectively. The borders, however, were not so clear because the difference is close to the threshold for Gly19 (−0.31 ppm), Arg29 (−0.47 ppm), Cys83 (−0.40 ppm), and Gly84 (+0.93 ppm). Thus the secondary structure including these residues will be modified taking into account the following hydrogen exchange study and will be shown in the next section.

Hydrogen-Deuterium Exchange—Figure 3 shows the $^1H\{^{15}N\}$HSQC spectrum obtained immediately after the temperature was raised from 10 to 52°C in deuterium oxide, pH* 6.14, in which 35 remaining cross peaks were observed. Among them, the signal for Asp83 was excluded from the following analysis because it overlaps with another signal. At pH* 6.14, the exchange was previously shown to follow the EX2 mechanism (*39*). Typical time courses of cross peak intensities are shown in Fig. 4. Similar experiments were carried out at pH* 8.96, where the exchange mechanism is supposed to be EX1 (*39*), although detection was started after incubating the protein solution for 12 h at 42°C in order to exchange out easily exchangeable protons. The measured exchange rates at pH* 6.14 were transformed to protection factors by taking into account the sequence dependence of the intrinsic exchange rate (*37*). Individual k_{int}/k_{ex} ratios were obtained at both pH* values (Table I) and are plotted in Fig. 5. At pH* 6.14, ΔG°_{HX} values were derived according to Eq. 4 and are shown in the last column of Table I.

Since the NH hydrogens observed here should form hydrogen bonds and are likely to be involved in secondary structures, we determined the secondary structure in solution according to the following criteria. (i) CSI is the

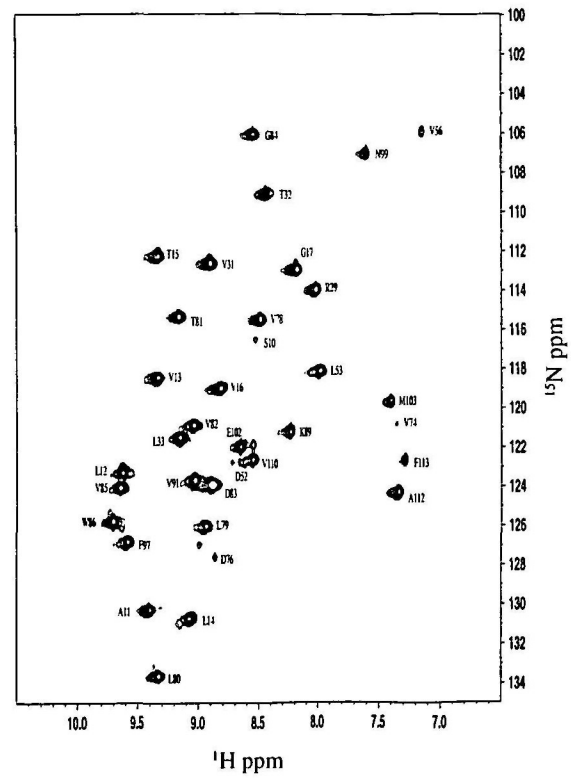

Fig. 3. **The amide region of the $^1H\{^{15}N\}$HSQC spectrum of uniformly ^{15}N-labeled SSI in deuterated phosphate buffer, pH* 6.14, at 52°C.** The signals were accumulated for 40 min immediately after the sample was brought to 52°C from 10°C.

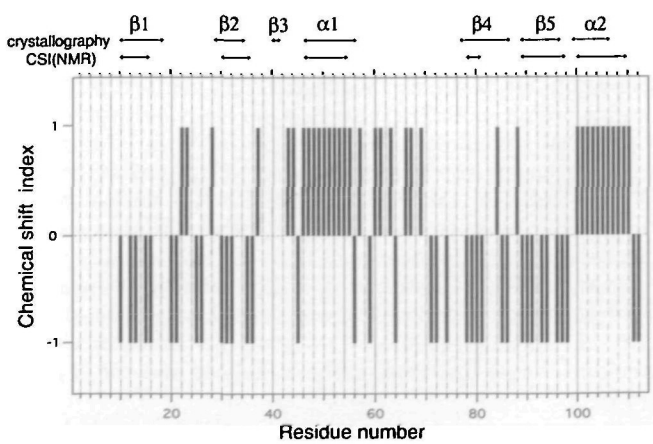

Fig. 2. **Chemical shift index plotted for the amino acid sequence of SSI.** Secondary structures determined by X-ray crystallography and Chemical Shift Index (CSI) are indicated at the top.

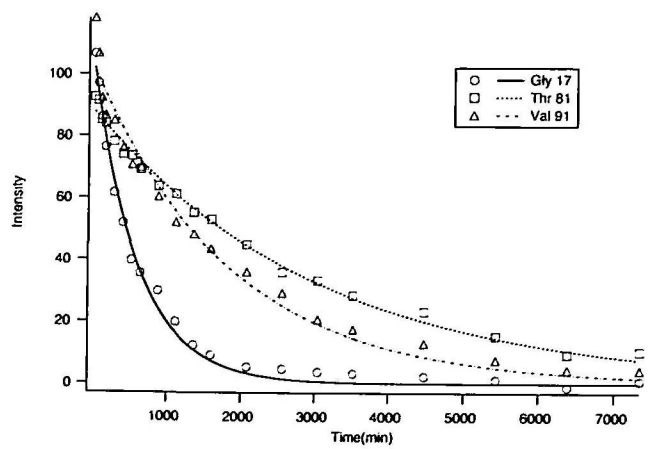

Fig. 4. **Time course of the signal intensities of the amide protons of Gly17 (○), Thr81 (□), and Val91 (△) measured at 52°C and pH* 6.14.** The curves were obtained by non-linear least-squares fitting of the experimental data to single exponential functions of time.

TABLE I. **k_{ex} and k_{int}/k_{ex} values of the main chain amide protons of *Streptomyces* subtilisin inhibitor at pH 6.14 and pH 8.95 at 52°C.**

Residue No.	k_{ex} at pH 6.14 52°C (min^{-1})	k_{ex} at pH 8.96 52°C (min^{-1})	k_{int}/k_{ex} at pH 6.14 52°C	k_{int}/k_{ex} at pH 8.96 52°C	$\Delta G°_{HX}$ at pH 6.14 52°C (kcal/mol)
Ser10	2.5e-03	N.D.	2.4e+05	N.D.	8.01
Ala11	5.7e-03	N.D.	1.5e+05	N.D.	7.73
Leu12	5.5e-04	5.1e-03	2.1e+05	1.8e+07	7.93
Val13	2.7e-04	3.9e-03	2.1e+05	1.1e+07	8.03
Leu14	4.9e-04	4.6e-03	1.7e+05	1.5e+07	7.80
Thr15	1.1e-03	5.1e-03	2.0e+05	3.6e+07	7.91
Val16	6.5e-04	6.2e-03	2.2e+05	1.8e+07	7.94
Gly17	1.7e-03	2.0e-03	3.6e+05	2.3e+08	8.27
Arg29	9.7e-03	N.D.	1.4e+05	N.D.	7.64
Val31	3.6e-04	4.3e-03	2.5e+05	1.6e+07	8.03
Thr32	5.4e-03	N.D.	5.1e+04	N.D.	7.01
Leu33	7.3e-04	4.7e-03	2.5e+05	3.1e+07	8.05
Asp52	1.3e-02	N.D.	1.7e+05	N.D.	7.78
Leu53	3.6e-03	N.D.	1.3e+05	N.D.	7.61
Val56	1.1e-01	N.D.	8.3e+02	N.D.	4.34
Val74	7.9e-02	N.D.	1.5e+03	N.D.	4.71
Asp76	7.4e-02	N.D.	3.3e+04	N.D.	6.73
Val78	8.3e-05	1.3e-03	6.1e+05	3.1e+07	8.62
Leu79	1.1e-04	2.5e-03	7.5e+05	2.7e+07	8.75
Leu80	1.4e-04	2.7e-03	5.1e+05	2.1e+07	8.50
Thr81	3.3e-04	4.3e-03	7.0e+05	4.3e+07	8.71
Val82	3.7e-04	4.7e-03	3.8e+05	2.4e+07	8.30
Asp83	N.D.	N.D.	N.D.	N.D.	N.D.
Gly84	6.1e-03	N.D.	5.4e+05	N.D.	8.54
Val85	3.8e-04	N.D.	3.4e+05	N.D.	8.25
Trp86	5.1e-04	N.D.	2.5e+05	N.D.	8.03
Lys89	1.7e-02	N.D.	3.6e+04	N.D.	6.79
Val91	5.5e-04	N.D.	2.7e+05	N.D.	8.08
Phe97	3.2e-04	4.4e-03	5.7e+05	3.4e+07	8.58
Asn99	2.7e-02	N.D.	1.0e+05	N.D.	7.46
Glu102	3.7e-02	N.D.	7.5e+04	N.D.	7.26
Met103	1.9e-02	N.D.	5.5e+04	N.D.	7.06
Val110	6.9e-03	N.D.	2.6e+04	N.D.	6.57
Ala112	1.3e-02	N.D.	3.8e+04	N.D.	6.83
Phe113	3.2e-02	N.D.	8.1e+03	N.D.	5.82

N.D. indicates that reliable integration was not obtained either due to a rapid loss of signal intensities or to the overlapping of signals.

basis. (ii) For residues Gly19, Arg29, Cys83, and Gly84, which were close to the threshold of the CSI criteria as mentioned in the previous section, hydrogens with detectable exchange rates were regarded as coming from participating residues in the secondary structure if they were consecutive. Then the resulting secondary structures determined by NMR were β1, β2, α1, β4, β5, and α2 for residues 10-17, 29-36, 46-56, 78-86, 89-98, and 100-110, respectively (Fig. 5).

DISCUSSION

CSI and Secondary Structure—According to the results of CSI (Fig. 2), the location and elements of the secondary structures showed several differences from those predicted by X-ray crystallography (*4*). (i) The β3-strand is completely missing. (ii) The α2-helix is longer in the C-terminal direction. Although the α2-helix was defined for Glu100 to Gly107 in the crystal structure, the α2-helix was determined to comprise Glu100 to Val110 by CSI. (iii) The ending positions for β1, β2, α1, β4, and β5 are slightly different from those in the crystal structure. (iv) The starting positions for β2 and β4 do not coincide with those

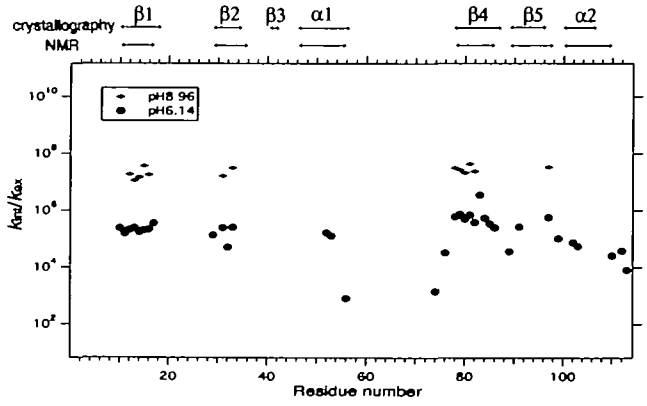

Fig. 5. **k_{int}/k_{ex} values of the amide protons of SSI at pH* 6.14 and pH* 8.96 at 52°C.** Secondary structures determined by X-ray crystallography and NMR based on CSI and hydrogen exchange experiments are indicated at the top.

in the crystal structure. Based on the present analysis with CSI, it is likely that SSI forms a dimeric interface consisting of a four-stranded β-sheet instead of a five stranded β-sheet as previously reported in the crystal (*4*). Recently, a newly refined crystallographic structure of SSI by X-PLOR (*40*) using the same diffraction data of Mitsui *et al.* (*4*) was reported (Protein Data Bank: 3SSI); this predicts a four-stranded β-sheet. These results appear to indicate that a stable existence is questionable for the five-stranded β-sheet. Although the refined crystal structure is in qualitative agreement with regard to the β-sheet structure, it also shows differences from the NMR CSI structure in solution in the many details mentioned above. Differences between the solution structure and the crystal structure (*4*) were reported earlier in terms of the microscopic environment of Tyr75 (*19*).

Hydrogen Exchange and Secondary Structure—The measurement of hydrogen exchange rates in proteins has become a useful tool for studying the structure, folding, and intermolecular interactions of proteins in solution (*41-43*). Although details of the mechanism of exchange and its quantitative correlation with structure and internal mobility are still not fully understood, various models agree upon a general two-process model (*44*). According to this model, there are two pathways for exchange: (i) exchange from the unstructured ensemble of the protein after global unfolding, and (ii) exchange by local fluctuations within the native ensemble. It has been suggested that while the buried amide protons of SSI in the core β-sheet are only exchanged by global unfolding, two α-helices and the C-terminal region exchange by local fluctuation (*39*). According to the X-ray analysis, the SSI subunit has 38 amide groups involved in hydrogen bonding with carbonyls, among which 25 belong to the β-sheet and 11 to the two α-helices. It is also known from IR studies that the exchange of the amide hydrogens can be classified into three kinetic classes with 72, 15, and 17 residues, the latter 32 slow exchanging residues being involved in the α-helices and the β-sheet (*45*).

In our experiment at pH* 6.14 and 52°C in ^2H_2O, we successfully identified thirty-five amide proton signals remaining for at least forty minutes as shown in Fig. 3. The amide protons involved in 17 hydrogen-bonds determined

by X-ray diffraction (Gly19, Thr24, Thr34, Cys35, Ser40, Thr42, Cys50, Ala51, Ala54, Ala55, Gly57, Ala62, Gln87, Tyr93, Asn104, Ala105, and His106) were exchanged rapidly before signal detection, while 8 peptide NH protons with no reported hydrogen bonding in the crystal structure (Gly17, Thr32, Val74, Asp76, Asn99, Val110, Ala112, Phe113) exchanged slowly with detectable signals. Among the 17 rapidly exchanging hydrogen bonded residues, Cys35, Ala51, Gly57, Gln87, and Ala105 have a non-zero accessible surface area for NH groups according to the crystallography (*4*). Even though the remnants of these residues have zero accessible surface areas and thus are completely buried inside the protein in the crystal structure (*4*), no signals were observed in the HSQC spectrum after 40 min of signal accumulation. Particularly, there were no observed signals from the β3-strand, indicating that the β3-strand is unstable or does not exist at all. Among the eight slowly exchanging amide protons that have been reported to be non-hydrogen bonded in the crystal structure (*4*), only Gly17 and Thr32 are located within the β-strand. The rest of the residues do not belong to any secondary structures in the crystal structure (*4*). From the observed slow exchange rates, the C-terminal residues, Val110, Ala112, and Phe113, are likely to be involved in some kind of secondary structure, while Asn99 might serve as an N-cap of the α2-helix. It is interesting to find that the hydrogen exchange rate is slow for Val74, which is located at the reactive site of the inhibitor and exposed to solvent (*2*), suggesting that it is involved in some kind of inter-residue interaction with the rest of the protein. This also explains why the pK_a value of Tyr75 is unusually high, 11.8, implying that its side chain might be involved in hydrogen bonding (*19*), although in the crystal this side chain is reported to be well exposed (*46*). In the refined crystal structure, no β3-strand is reported and the α2-helix extends to Asn104. Our hydrogen exchange experiments show better agreement with the refined crystal structure, although there are still some discrepancies.

Hydrogen Exchange Kinetics and Global Stability—When hydrogen exchange occurs in the EX2 mechanism at pH* 6.14 (*39*), the k_{int}/k_{ex} ratios indicate the protection factor P (Eq. 3), whereas at pH* 8.96, where EX1 mechanism prevails (*39*), they represent rates of unfolding (Eq. 5) and not K_{op}. Thus the differences in the absolute values of the exchange rates between the two pH*s shown in Fig. 5 are caused by the difference in the exchange mechanism. Since all the easily exchangeable protons were replaced with deuterons beforehand at pH* 8.96 and the remaining thirteen protons (Leu12, Val13, Leu14, Thr15, and Val16 in the β1 strand, Val31 and Leu33 in the β2 strand, Val78, Leu79, Leu80, Thr81, and Val82 in the β4 strand, and Phe97 in the β5 strand; note that Asp83 is observed but excluded due to signal overlapping) show similar ratios, these rates are likely to represent the frequency of the global unfolding event. It is to be noted that all these residues are located at the interface of the dimeric interaction consisting of the β-sheet.

For quantitative analysis of the global unfolding at atomic resolution, exchange rates at pH* 6.14 for signals remaining even at pH* 8.96 were obtained. As shown in Fig. 5, the protection factors (P) for these 13 residues are close to each other at pH* 6.14. The average protection factor for these residues is 3.9×10^5 or the average $\Delta G^\circ_{HX}=8.2$ kcal/mol (Table I) at 42°C. At this temperature the free energy of equilibrium thermal unfolding, which has been proven to be a cooperative phenomenon without the accumulation of any native-like monomer or intermediate (*7*), can be precisely calculated based on thermodynamic parameters calorimetrically obtained (*13*). This was made possible by making the best use of the precise values of the enthalpy change (120.9 kcal/mol at 60°C) and the heat capacity change upon unfolding, ΔC_p, which itself is a function of temperature, *i.e.*, $C_p^N=0.0483T+6.86$ (kcal/mol/°C), $C_p^U=-0.000314T^2+0.0592T+9.94$ (kcal/mol/°C) and $\Delta C_p=C_p^U-C_p^N$ (*13*), in a temperature range from 15 to 105°C. Based on these parameters, the free energy was determined to be 17.0 kcal/mol per dimer, or 8.5 kcal/mol per monomer at 52°C. The latter value coincides very well with that obtained in the present hydrogen exchange study, $\Delta G^\circ_{HX}=8.2$ kcal/mol, implying that the global unfolding of the monomeric unit occurs without affecting the accompanying unit in the dimer. Although the value of the free energy itself can not distinguish the molecular mechanism of global unfolding, it is safe to say that the hydrogen exchange can be induced in the absence of complete unfolding of the dimer. This is in clear contrast with the fact that all attempts to dissociate the native dimer into native monomers by mutations in equilibrium studies have failed so far (*15*).

Although all the amide protons in the slowly exchanging groups exchange at similar rates at pH* 8.96, suggesting that they exchange by global unfolding, at pH* 6.14 the protection factors for residues in the β4-strand, especially Val78, Leu79, and Thr81, are slightly higher than those of the rest (Table I, Fig. 5), implying that this region is highly resistant to local unfolding and thus might serve as a folding core (*41*).

Local Stability—In addition to the global unfolding event detected for the remaining 14 residues at pH* 8.96, as described in the previous section, local unfolding can be detected as differences in k_{int}/k_{ex}. Two differences are noted in the exchange rates between the data at pH* 6.14 and 8.96 (Fig. 5). One is an acceleration of the exchange rate for the α1- and α2-helices and for the three C-terminal residues at pH* 8.96, suggesting enhanced local fluctuations in these parts of the molecule at 52°C. The other is the observation of faster exchange rates at pH* 8.96 for residues in the β2 and β5 strands, suggesting local fluctuations in these β-strands. Although CSI does not suggest any specific secondary structure for the C-terminal residues (Ala112 and Phe113), the moderate exchange rates at pH* 6.14 for these residues suggest that this region lies in a structurally stable part of the molecule. This finding is consistent with the fact that SSI-A (SSI with the four C-terminal residues removed) is markedly less stabile than intact SSI (*2*).

The differences in P at the same pH* value of 6.14, notably P values lower than 5×10^4 for Val56, Val74, Asp76, Leu79, Lys89, Val110, Ala112, and Phe113, should also be caused by local fluctuations. Among them, Val74, Asp76, Leu79, Val110, Ala112, and Phe113 do not participate in the formation of any secondary structure in the crystal (*4*), and thus it is likely that the hydrogen networks are weakly held. Other residues involved in the secondary structures without detectable protection factors are mainly

located in the $\alpha 1$ and $\alpha 2$ helices, and $\beta 2$ and $\beta 3$ strands, suggesting that these secondary structures have some modes of local fluctuation and/or solvent accessibility. In other words,the $\beta 1$ and $\beta 4$ sheets are tightly packed and form a well-organized secondary structure. This may be because the two strands are the central strands in the β-sheet comprising the $\beta 2$, $\beta 1$, $\beta 4$, and $\beta 5$ strands according to our present NMR data and the recent refined crystallographic structure.

We believe that these evaluations of local as well as global unfolding derived from hydrogen exchange for individual residues provide an invaluable source for future folding studies of this protein with a unique dimeric structure.

REFERENCES

1. Murao, S. and Sato, S. (1972) S-SI, a new alkaline protease inhibitor from *Streptomyces albogriseolus* S-3253. *Agric. Biol. Chem.* **36**, 1737-1744
2. Hiromi, K., Akasaka, K., Mitsui, Y., Tonomura, B., and Murao, S. (1985) *Protein Protease Inhibitor—The Case of Streptomyces Subtilisin Inhibitor*, Elsevier, Amsterdam
3. Satow, Y., Mitsui, Y., and Iitaka, Y. (1978) Crystal structure of a protein proteinase inhibitor, SSI (*Streptomyces* subtilisin inhibitor), at 4 Å resolution. *J. Biochem.* **84**, 897-906
4. Mitsui, Y., Satow, Y., Watanabe, Y., and Iitaka, Y. (1979) Crystal structure of a bacterial protein proteinase inhibitor (*Streptomyces* subtilisin inhibitor) at 2.6 Å resolution. *J. Mol. Biol.* **131**, 697-724
5. Takeuchi, Y., Satow, Y., Nakamura, K.T., and Mitsui, Y. (1991) Refined crystal structure of the complex of subtilisin BPN′ and *Streptomyces* subtilisin inhibitor at 1.8 Å resolution. *J. Mol. Biol.* **221**, 309-325
6. Takahashi, K. and Sturtevant, J.M. (1981) Thermal denaturation of *Streptomyces* subtilisin inhibitor, subtilisin BPN′ and the inhibitor-subtilisin complex. *Biochemistry* **20**, 6185-6190
7. Tamura, A., Kojima, S., Miura, K., and Sturatevant, J.M. (1994) Effect of an intersubunit disulfide bond on the stability of *Streptomyces* subtilisin inhibitor. *Biochemistry* **33**, 14512-14520
8. Takeuchi, Y., Noguchi, S., Satow, Y., Kojima, S., Kumagai, I., Miura, K., Nakmura, K.T., and Mitsui, Y. (1991) Molecular recognition at the active site of subtilisin BPN′: crystallographic studies using genetically engineered proteinaceous inhibitor SSI (*Streptomyces* subtilisin inhibitor). *Protein Eng.* **4**, 501-508
9. Takeuchi, Y., Nonaka, T., Nakamura, K.T., Kojima, S., Miura, K., and Mitsui, Y. (1992) Crystal structure of an engineered subtilisin inhibitor complexed with bovine trypsin. *Proc. Natl. Acad. Sci. USA* **89**, 4407-4411
10. Tamura, A., Kimura, K., and Akasaka, K. (1991) Cold denaturation and heat denaturation of *Streptomyces* subtilisin inhibitor. 2. ^{1}H NMR studies. *Biochemistry* **30**, 11313-11320
11. Tamura, A., Kimura, K., Takahara, H., and Akasaka, K. (1991b) Cold denaturation and heat denaturation of *Streptomyces* subtilisin inhibitor.1. CD and DSC studies. *Biochemistry* **30**, 11307-11313
12. Konno, T., Kataoka, M. Kamatari, Y., Kanaori, K., Nosaka, A., and Akasaka, K. (1995) Solution X-ray scattering analysis of cold-, heat-, and urea-denatured states in a protein, *Streptomyces* subtilisin inhibitor. *J. Mol. Biol.* **251**, 95-103
13. Tamura, A. and Privalov, P.L. (1997) The entropy cost of protein association. *J. Mol. Biol.* **273**, 1048-1060
14. Tamura, A. (1998) Mutational effects on cold denaturation and hydration of a protein, *Streptomyces* subtilisin inhibitor. *Thermochim. Acta* **308**, 35-40
15. Tamura, A., Kojima, S., Miura, K., and Sturtevant, J.M. (1995) A thermodynamic study of mutant forms of *Streptomyces* subtilisin inhibitor. II. Replacements at the interface of dimer formation, Val13. *J. Mol. Biol.* **249**, 636-645
16. Tamura, A. and Sturtevant, J.M. (1995) A thermodynamic study of mutant forms of *Streptomyces* subtilisin inhibitor. I. Hydrophobic replacements at the position of Met103. *J. Mol. Biol.* **249**, 625-635
17. Tamura, A. and Sturtevant, J.M. (1995) A thermodynamic study of mutant forms of *Streptomyces* subtilisin inhibitor. III. Replacements of a hyper-exposed residue, Met73. *J. Mol. Biol.* **249**, 646-653
18. Komiyama, T. and Miwa, M. (1980) Fluorescence quenching as an indicator for the exposure of tryptophyl residues in *Streptomyces* subtilisin inhibitor. *J. Biochem.* **87**, 1029-1036
19. Fujii, S., Akasaka, K., and Hatano, H. (1981) Proton magnetic resonance study of *Streptomyces* subtilisin inhibitor. pH titration and assignment of individual tyrosyl resonances. *Biochemistry* **20**, 518-523
20. Akasaka, K., Fujii, S., and Kaptein, R. (1981) Exposure of aromatic residues of *Streptomyces* subtilisin inhibitor. A photo-CIDNP study. *J. Biochem.* **89**, 1945-1949
21. Akasaka, K., Fujii, S., and Hatano, H. (1982a) Dynamic state of the three methionyl residues of *Streptomyces* subtilisin inhibitor. ^{1}H NMR studies. *J. Biochem.* **92**, 591-598
22. Akasaka, K., Hatano, H., Tsuji, T., and Kainosho, M. (1982b) Proton magnetic resonance study of the tryptophan residue of *Streptomyces* subtilisin inhibitor. *Biochim. Biophys. Acta* **704**, 503-508
23. Kainosho, M. and Tsuji, T. (1982) Assignment of the three methionyl carbon resonances in *Streptomyces* subtilisin inhibitor by a carbon-13 and nitrogen-15 double-labeling technique. A new strategy for structural studies of proteins in solution. *Biochemistry* **21**, 6273-6279
24. Kainosho, M., Nagao, Y., Imamura, K., Uchida, N., Tomonaga, Y., and Tsuji, T. (1985) Structure studies of a protein using the assigned back-bone carbonyl carbon-13 NMR resonance. *J. Mol. Struct.* **126**, 549-562
25. Sasakawa, H., Tamura, A., Akasaka, K., Taguchi, S., Miyake, Y., and Kainosho, M. (1999) Backbone ^{1}H, ^{13}C, and ^{15}N resonance assignments of *Streptomyces* subtilisin inhibitor. *J. Biomol. NMR* **14**, 285-286
26. Inoue, T. and Akasaka, K. (1987) Self association of *Streptomyces* subutilisin inhibitor: sedimentation equilibrium and ^{1}H NMR studies. *J. Biochem.* **102**, 1371-1378
27. Englander, S.W., Sosnick, T.R., Englander, J.J., and Mayne, L. (1996) Mechanisms and uses of hydrogen exchange. *Curr. Opin. Struct. Biol.* **6**, 18-23
28. Jia, X., Reisman, J.M., Hsu, V.L., Geiduschek, E.P., Parello, J., and Kearns, D.R. (1994) Proton and nitorogen NMR sequence-specific assignments and secondary structure determination of the *Bacillus subtilis* SPO1-enhanced transcription factor 1. *Biochemistry* **33**, 8842-8852
29. Junius, F.K., Mackay, J.P., Bubb, W.A., Jesen, S.A., Weiss, A.S., and King, G.F. (1995) Nuclear magnetic resonance characterization of the jun leucine zipper domain: unusual properties of coliled-coil interfacial polar residues. *Biochemistry* **34**, 6164-6174
30. Kay, L.E., Ikura, M., Tschudin, R., and Bax, A. (1990) Three-dimensional triple-resonance NMR spectroscopy of isotopically enriched proteins. *J. Magn. Reson.* **89**, 496-514
31. Kay, L.E., Xu, G.Y., and Yamazaki, T. (1994) Enhanced-sensitivity triple-resonance spectroscopy with minimal H_2O saturation. *J. Magn. Reson.* **109**, 129-133
32. Piotto, M., Saudek, V., and Sklenar, V. (1992) Gradient-tailored excitation for single-quantum NMR spectroscopy of aqueous solution. *J. Biomol. NMR* **2**, 661-665
33. Delaglio, F., Grzesiek, S., Vuister, G.W., Zhu, G., Pfeifer, J., and Bax, A. (1995) NMRPipe: A multidimensional spectral processing system based on UNIX pipes. *J. Biomol. NMR* **6**, 277-293
34. Cavanagh, J., Fairbrother, W.J., Palmer III, A.G., and Skelton, N.J. (1996) *Protein NMR Spectroscopy Principles and Practice*, Academic Press, San Diego
35. Bodenhausen, G. and Ruben, D.J. (1980) Natural abundance nitrogen-15 NMR enhanced heteronuclear spectroscopy. *Chem. Phys. Lett.* **69**, 185-189
36. Hvidt, A. and Nielsen, S.O. (1966) Hydrogen exchange in

proteins. *Adv. Protein Chem.* **21**, 287-386
37. Bai, Y., Milne, J.S., Mayne, L., and Englander, S.W. (1993) Primary structure effects on peptide group hydrogen exchange. *Proteins Strut. Func. Genet.* **17**, 75-86
38. Wishert, D.S. and Sykes, B.D. (1994) Chemical shifts as a tool of structure determination. *Methods Enzymol.* **239**, 363-392
39. Akasaka, K., Inoue, T., Hatano, H., and Woodward, C.K. (1985) Hydrogen exchange kinetics of core peptide protons in *Streptomyces* subtilisin inihibitor. *Biochemistry* **24**, 2973-2979
40. Brünger, A. (1992) *X-PLOR, A system for X-ray Crystallography and NMR*, Yale University Press, New Haven
41. Bai, Y., Sosnick, T.R., Mayne, L., and Englander, S.W. (1995) Protein folding intermediates: native-state hydrogen exchange. *Science* **269**, 192-197
42. Itzhaki, L.S., Neira, J., and Fersht, A.R. (1997) Hydrogen exchange in chymotrypsin inhibitor 2 probed by denaturants and temperature. *J. Mol. Biol.* **270**, 89-98
43. Laura, J., Itzhaki, S., Otzen, D.E., Davis, B., and Fersht, A. (1997) Hydrogen exchange in chymotrypsin inhibitor 2 probed by mutagenesis. *J. Mol. Biol.* **270**, 99-110
44. Englander, S.W. and Mayo, L. (1992) Protein folding studied using hydrogen-exchange labeling and two-dimensional NMR. *Annu. Rev. Biophys. Biomol. Struct.* **21**, 243-265
45. Nakanishi, M. and Tsuboi, M. (1976) Structure and fluctuation of a *Streptomyces* subtilisin inhibitor. *Biochim. Biophys. Acta* **434**, 365-376
46. Satow, Y., Watanabe, Y., and Mitsui, Y. (1980) Solvent accessibility and microenvironment in a bacterial protein proteinase inhibitor SSI (*Streptomyces* subtilisin iinhibitor). *J. Biochem.* **88**, 1739-1755
47. Kraulis, P.J. (1991) MOLSCRIPT—A program to produce both detailed and schematic plots of protein structure. *J. Appl. Crystallogr.* **24**, 946-950